University of New Hampshire
University of New Hampshire Scholars' Repository

Master's Theses and Capstones | Student Scholarship

Fall 2018

# FOUR YEARS OF UNMANNED AERIAL SYSTEM IMAGERY REVEALS VEGETATION CHANGE IN A SUB-ARCTIC MIRE DUE TO PERMAFROST THAW

Jessica DelGreco
*University of New Hampshire, Durham*

Follow this and additional works at: https://scholars.unh.edu/thesis

Recommended Citation
DelGreco, Jessica, "FOUR YEARS OF UNMANNED AERIAL SYSTEM IMAGERY REVEALS VEGETATION CHANGE IN A SUB-ARCTIC MIRE DUE TO PERMAFROST THAW" (2018). *Master's Theses and Capstones*. 1216.
https://scholars.unh.edu/thesis/1216

This Thesis is brought to you for free and open access by the Student Scholarship at University of New Hampshire Scholars' Repository. It has been accepted for inclusion in Master's Theses and Capstones by an authorized administrator of University of New Hampshire Scholars' Repository. For more information, please contact nicole.hentz@unh.edu.

# FOUR YEARS OF UNMANNED AERIAL SYSTEM IMAGERY REVEALS VEGETATION CHANGE IN A SUB-ARCTIC MIRE DUE TO PERMAFROST THAW

By

JESSICA LYNN DELGRECO

Environmental Science: Ecosystems (BS), University of New Hampshire, 2016

THESIS

Submitted to the University of New Hampshire

in Partial Fulfillment of

the Requirements for the Degree of

Master of Science

In

Earth Science: Geochemical Systems

September, 2018

This thesis has been examined and approved in partial fulfillment of the requirements for the degree of Master of Science in Earth Science: Geochemical Systems by:

Thesis Director, Michael Palace,
Associate Professor,
Earth Systems Research Center
Department of Earth Sciences
University of New Hampshire

Ruth K. Varner,
Professor,
Earth Systems Research Center
Department of Earth Sciences
University of New Hampshire

Steve Frolking,
Research Professor,
Earth Systems Research Center
University of New Hampshire

On June 21, 2018

Original approval signatures are on file with the University of New Hampshire Graduate School.

TABLE OF CONTENTS

ACKNOWLEDGEMENTS ..... IV
LIST OF TABLES ..... V
LIST OF FIGURES ..... VI
ABSTRACT ..... VII
1. INTRODUCTION ..... 1
2. METHODS ..... 6
*2.1 Study site* ..... 6
*2.2 Temperature and Precipitation Data* ..... 7
*2.3 Vegetation Cover at Stordalen Mire* ..... 7
*2.4 UAS Image Data Collection* ..... 10
*2.5 Georectification* ..... 11
*2.6 Vegetation Plot Data Collection* ..... 12
*2.7 UAS Image Classification* ..... 13
*2.8 Estimating Land Cover Change via Classification Maps* ..... 16
3. RESULTS ..... 18
*3.1 UAS Imagery Data Collection* ..... 18
*3.2 UAS Image Classifications* ..... 19
*3.3 Error analysis and cover class assessment* ..... 22
*3.5 Quantification of Land Cover Change* ..... 24
*3.6 Temperature and Precipitation Trends* ..... 25
4. DISCUSSION ..... 27
*4.1 UAS Image Processing and Classification* ..... 27
*4.2 Vegetation Changes* ..... 28
*4.3 Implications on the Carbon Balance* ..... 34
*4.5 Estimation of Land Cover Change* ..... 34
*4.6 Future Work* ..... 34
5. CONCLUSION ..... 36
6. BIBLIOGRAPHY ..... 37

ACKNOWLEDGEMENTS

We would like to thank the Abisko Scientific Research Station for access to the Stordalen Mire and for laboratory space and housing. Also, thank you to Clarice Perryman, Chris Horruitiner and Apryl Perry for assistance during flights. This research was supported through two grants from the National Science Foundation to R. Varner: Northern Ecosystems Research for Undergraduates REU site (EAR#1063037) and MacroSystems Biology grant (EF #1241037). This research was also funded by the University of New Hampshire's Summer Undergraduate Research Fellowship (SURF) Abroad (to J. DelGreco), the New Hampshire NASA EPSCoR RID Space Grant (to J. DelGreco), and the University of New Hampshire's Earth Science Department travel grant (to J. DelGreco).

LIST OF TABLES

Table 1: Species Composition Characteristic of Each Vegetation Cover Type

Table 2: Cover Type Groupings Based on Permafrost Thaw Stage

Table 3: Vegetation Classification Error Matrices 2014 – 2017

Table 4: Estimation of Permafrost Dynamics 2014 – 2017

LIST OF FIGURES

Figure 1: Study Site, Stordalen Mire Abisko, Sweden

Figure 2: Vegetation Cover Type Classification

Figure 3: Random Point Vegetation Sampling Scheme

Figure 4: Vegetation Plots - Classification Process

Figure 5: Training and Validation for Cover Classification for a Random Forest Classifier

Figure 6: 2014 UAS Imagery Cover Type Classification

Figure 7: Classification Maps Comparison: 3 cm Resolution vs 12 cm Resolution

Figure 8: Percent Cover Change across Stordalen Mire 2014 – 2017

Figure 9: Monthly Average Air Temperature at Stordalen Mire 2014-2017

Figure 10: Monthly Total Precipitation at Stordalen Mire 2014-2017

Figure 11: Visual Representation of Landscape Changes 2014-2017

ABSTRACT

FOUR YEARS OF UAS IMAGERY REVEALS VEGETATION CHANGE IN A SUB-ARCTIC MIRE DUE TO PERMAFROST THAW

by

Jessica DelGreco

University of New Hampshire, September, 2018

Warming trends in sub-arctic regions have resulted in thawing of permafrost which in turn induces change in vegetation across peatlands both in areal extent and composition. Collapse of palsas (i.e. permafrost plateaus) has also been correlated with increases in methane ($CH_4$) emission to the atmosphere. Vegetation change provides new microenvironments that promote $CH_4$ production and emission, specifically through plant interactions and structure. By quantifying the changes in vegetation at the landscape scale, we will be able to scale the impact of thaw on $CH_4$ emissions in these complex climate-sensitive northern ecosystems. We combine field-based measurements of vegetation composition and Unmanned Aerial Systems (UAS) high resolution (3 cm) imagery to characterize vegetation change in a sub-arctic mire. The objective of this study is to analyze how vegetation from Stordalen Mire, Abisko, Sweden, has changed over time in response to permafrost thaw. At Stordalen Mire, we flew a fixed-wing UAS in July of each of four years, 2014 through 2017, over a 1 km x 0.5 km area. High precision GPS ground control points were used to georeference the imagery. Randomized square-meter plots were measured for vegetation composition and individually classified into one of five vegetation cover types, each representing a different stage of permafrost degradation. Using these training data, each year of imagery was classified by cover type in Google Earth Engine using a Random

Forest Classifier. Textural information was extracted from the imagery, which provided additional spatial context information and improved classification accuracy. Twenty five percent of the training data were held back from the classification and used for validation, while the remaining seventy five percent of the training data were used to classify the imagery. The overall classification accuracy for 2014-2017 was 80.6%, 79.1%, 82.0%, and 82.9%, respectively. Percent cover across the landscape was calculated from each classification map and compared between years. Hummock sites, representing intact permafrost, decreased coverage by 9% from 2014-2017, while semi-wet sites increased coverage by 18%. This four-year comparison of vegetation cover indicated a rapid response to permafrost thaw. The use of a UAS allowed us to effectively capture the spatial heterogeneity of a northern peatland ecosystem. Estimation of vegetation cover types is vital in our understanding of the evolution of northern peatlands and their future role in the global carbon cycle.

# 1. INTRODUCTION

Warming trends in sub-arctic regions are resulting in permafrost thaw, which is causing changes to plant communities and emissions of radiatively important trace gases. Arctic and sub-arctic regions are highly vulnerable to climate change as they are expected to experience greater warming than anywhere else on the globe (Kattsov et al., 2005 in ACIA, 2005, IPCC senarios A2 and B2). In these arctic regions, increases in global temperatures have caused and are continuing to cause thawing of permafrost peatlands (permanently frozen ground). Mean annual air temperature has increased by 2.5°C from 1913 to 2006, exceeding the 0°C threshold. Historically, mean annual temperatures have been below 0°C, above which permafrost is particularly vulnerable (Callaghan et al., 2010). Permafrost thaw has various implications from altering ecosystem dynamics to increasing greenhouse gas emissions (Deng et al., 2014, Christensen et al., 2004, Torbick et al., 2012). It is important to study these northern permafrost peatland ecosystems to better understand their role in global climate change and emission of radiatively important gases.

Northern permafrost peatlands have been recognized as being a large stock for soil carbon, however, as permafrost thaw progresses these ecosystems may become a source of carbon to the atmosphere (Billings et al., 1982). Permafrost peatland soils currently hold 20-30% of all global soil organic carbon (Hugelius et al., 2014). The ability of these permafrost peatlands to act as a carbon-sink and accumulate organic carbon is due to high productivity and low decomposition rates (Bäckstrand et al., 2010). However, as permafrost thaws, soil carbon is available for decomposition and potentially released to the atmosphere as greenhouse gases (methane ($CH_4$) and carbon dioxide ($CO_2$)). These greenhouse gases are of concern as emissions

can cause positive feedbacks creating a warmer climate, thus increasing permafrost thaw (Christensen et al., 2004). Analyzing the changing permafrost dynamics proves vital in quantifying the global carbon system.

Permafrost thaw influences vegetation composition, therefore changes in vegetation distribution can be used as a proxy for assessing permafrost dynamics. Vegetation composition is impacted through permafrost thaw via increases in the water table and deepening of the active layer (Deng et al., 2014). These vegetation changes provide new avenues of $CH_4$ release, specifically through plant structure (Malmer et al., 2005). Therefore, changes in vegetation distribution on thawing peatlands can be an indicator of changes in greenhouse gas exchange. Several studies on carbon fluxes from vegetation to the atmosphere have shown high variability in C fluxes due to differences in plant composition (Malmer et al., 2005; Bäckstrand et al., 2010; Johannsson et al., 2006; Deng et al., 2014; McCalley et al 2014). To understand the magnitude of $CH_4$ emissions in the northern regions, it is crucial to quantify vegetation at a landscape level.

A difficulty with estimating vegetation in the northern latitudes is the high spatial variability of the landscape, with species distribution change at scales of centimeters to meters. Therefore, grouping species into vegetation cover types provides a simplified classification scheme which can be scaled to sub-arctic regions. Malmer et al. (2005) provided a classification scheme that relates to plant functional types, the hydrological state of the landscape, and methane emissions. Each cover type represents a different stage of permafrost degradation, which is useful for estimating permafrost dynamics across the landscape. Shifts in cover types must be analyzed at the landscape level over time to understand how $CH_4$ emissions are changing across the landscape. To do so, it is essential to have appropriate tools that accurately measure the highly heterogeneous vegetation composition of the northern peatlands.

Remote sensing techniques have been used to map the vegetation of arctic regions, however there has been difficulty in capturing the heterogeneity due to low spatial resolution of satellites like MODIS and Landsat (Lees et al., 2018). With the coarse spatial resolution of satellite imagery, a single pixel may encompass a mixture of vegetation cover types, making it more difficult to estimate vegetation parameters (Matese et al., 2015). The use of high resolution optical satellites and lidar may provide insight into species composition at a large spatial coverage (Siewart 2018). High resolution satellite data collection, however can be very expensive and is still limited by the lack of spatial resolution that is needed in these highly variable northern ecosystem landscapes. Also, satellite imagery may be impacted by cloud cover (Anderson and Gaston, 2013) and have issues studying time specific processes, such as phenology, as temporal resolution can vary (Matese et al., 2015).

Plane-based airborne collection provides an opportunity to improve spatial resolution, but often at an inflated cost with limited collection periods. Aircraft based color infrared (CIR) images of Stordalen Mire, Abisko Sweden from 1970 and 2000 were compared to estimate vegetation changes using the previously described classification scheme (Malmer et al., 2005). Stordalen Mire is a discontinuous permafrost peatland ecosystem, and therefore highly heterogenous. The 1 m spatial resolution of the aerial CIR images may have resulted in loss of the fine-scale spatial heterogeneity, which may cause error in estimating permafrost degradation.

Unmanned Aerial Systems (UAS) have the potential to accurately characterize the high spatial variability of northern peatland ecosystems through the collection of high resolution imagery. The use of UASs for remote sensing in environmental studies is rapidly expanding in use (Anderson and Gaston, 2013). There has been a great deal of speculation about the benefits of using UAS imagery for ecological studies due to the limited spatial coverage and experience

required in deployment and flying (Anderson and Gaston, 2013). However, the use of a UAS provides a low cost, repeatable method for data collection (Matese et al., 2015). Image collection via UASs provide high spatial resolution without the issues of cloud cover. Coarser spatial resolution imagery, such as satellite imagery, will generally contain a mixture of vegetation cover types for an individual pixel, which increases the difficulty of accurately estimating vegetation cover (Lu, 2006). High resolution UAS imagery is therefore an effective tool for capturing small scale variations vegetation across a landscape.

Remotely sensed imagery can be classified into categories using a variety of machine learning techniques (Khatami et al., 2016; Gislason et al., 2006). Supervised classification techniques involve the analyst selecting samples sites with known class types, also known as training samples. The spectral properties of each pixel in the image are then compared to this training data to classify the whole image (Li et al., 2014). Many machine learning classification techniques have been developed including artificial neural network, classification tree, random forests, and support vector machine (Li et al., 2014). However, a Random Forest Classifier (RF) has been shown to most accurately classify vegetation across a landscape when used in conjunction with training data (Lawrence et al., 2006, Khatami et al., 2016). The RF Classifier creates sets of Classification and Regression Trees (CARTs) to make a prediction based on a randomly selected subset of the training set (Breiman, 2001). RF classifier does not overfit the model, which is a major issue with single classification trees such as CART (Lawrence et al., 2006). Also, it has been found that the RF classifier is more stable than a single classifier as it can handle large variations in the data (Belgiu and Drăguţ, 2016; Khatami et al., 2016).

Including textural analysis in imagery classification can improve the overall classification by providing additional spatial context information (Khatami et al. 2016; Soares et al. 1997).

Textural analysis relates to the spatial variation of image tone values (Franklin and Wulder, 2002) and is a technique used to improve image classification accuracy (Mongus and Žalik, 2018). The relationship between each pixel and its neighbors are examined and therefore additional properties about the image are determined (Soares et al., 1997). Studies have found that incorporating texture metrics improves image classification by removing confusion among classes that are spectrally similar (Franklin et al., 2000; Mongus and Žalik, 2018).

For this study, we developed a high resolution four-year UAS imagery analysis which incorporates textural components such as minimum, maximum, mean, standard deviation, entropy, angular secondary momentum, and evenness (Soares et al., 1997; Ouma et al., 2008). We used a RF Classifier to classify four years UAS imagery collected at Stordalen Mire, Abisko Sweden, from 2014 through 2017, to assess how vegetation dynamics have changed over time in response to permafrost thaw.

The objective of this study is to analyze vegetation changes in a sub-arctic mire through four years of high resolution 3 cm UAS imagery. At Stordalen Mire, Abisko Sweden, field measurements of vegetation composition were linked with each year of UAS imagery to classify vegetation distribution using a Random Forest Classifier. The Malmer et al. (2005) vegetation classification scheme was used to characterize the landscape which allows this work to be linked to ongoing studies. This multi-year study (2014-2017) allows for a robust and thorough assessment of thaw which may be otherwise attributed to interannual variability during our shorter period of study. Results from the comparison of vegetation distribution between years indicates a rapid response to permafrost thaw. It is also shown that high resolution imagery is needed to capture the heterogeneity among the landscape.

# 2. METHODS

## *2.1 Study site*

The study site, Stordalen Mire (68°21'N, 18°49'E), is located 10 km northeast of Abisko Scientific Research Station (Fig. 1). Stordalen Mire is in the sub-arctic region of discontinuous permafrost peatland ecosystems and has been rapidly undergoing permafrost thaw in the past decade. A mire is a wetland ecosystem, dominated by peat-forming plants. This heterogeneous discontinuous peatland region is characterized by close proximity variation in topography, hydrology, soil, and vegetation across the landscape (Deng et al. 2014). Research in Stordalen Mire has shown that sub-arctic peatland ecosystems have become wetter, which has led to changes in vegetation cover as well as changes in C fluxes (Christensen et al., 2004; Johansson et al. 2006). Stordalen Mire is a heavily researched study site and is an ideal location for this study as it encompasses vegetation relating to different stages of permafrost thaw.

Average annual temperature and precipitation was measured at the nearby Abisko Scientific Research Station. Mean annual temperature (MAT) increased by 2.5°C between 1913 and 2006 (Callaghan et al. 2010). This has led to mean annual temperatures above 0°C for the past few decades. Total precipitation from 1913–2009 was 306 mm and increased to 336 mm during the period 1980–2009 (Olefeldt and Roulet, 2012). The growing season is defined as the summer months with growing degree days above zero degrees Celsius (Christensen et al., 2004), which is generally from May-September (Johansson et al. 2006).

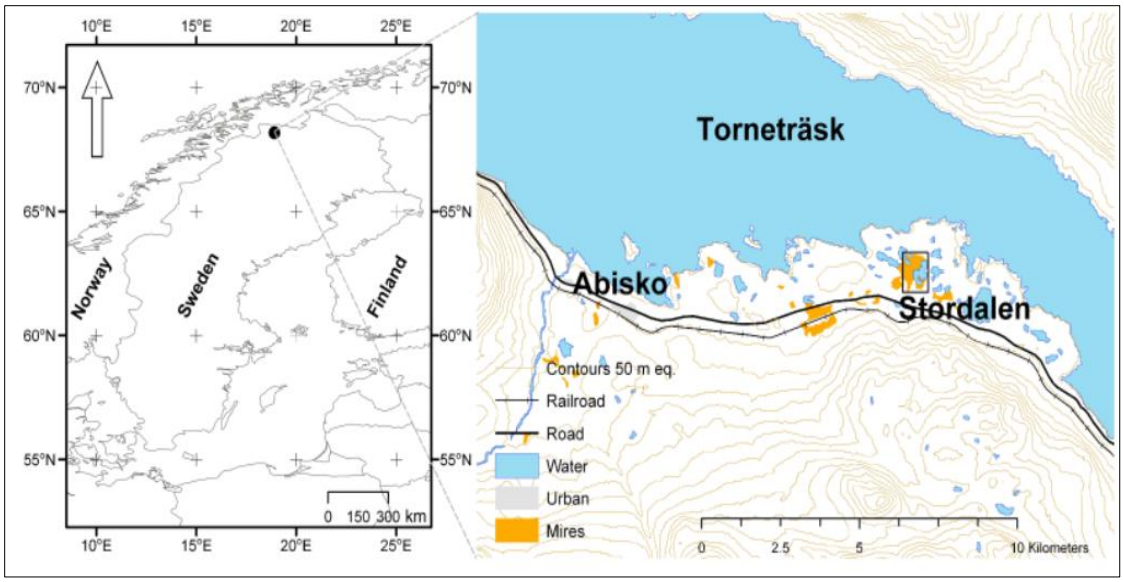


**Fig. 1.** Study site location in northern most Sweden (left) with an overview of the Abisko area showing Stordalen Mire (right). Adapted from "Decadal vegetation changes in a northern peatland, greenhouse gas fluxes and net radiative forcing," by T. Johannsson, N. Malmer, P. Crill, T. Friborg, J, Åkerman, M. Mastepanov, and T. Christensen, 2006, *Global Change Biology*, *12*(12). Copyright 2006 by The Authors.

## *2.2 Temperature and Precipitation Data*

Temperature and precipitation data was collected at Stordalen Mire from the ICOS Sweden station Abisko-Stordalen from 2014-2017 in ten-minute intervals. This ICOS Sweden Stordalen WeatherHawk 510 weather station is mounted 4m above the surface. The ten-minute data was averaged monthly for temperature and summed monthly for precipitation totals.

## *2.3 Vegetation Cover at Stordalen Mire*

Stordalen Mire is a highly heterogeneous peatland ecosystem consisting of vegetation cover types related to various stages of permafrost thaw. These cover types differ in plant functional types and the hydrological state of the landscape (Malmer et al., 2005). The five vegetative cover types used to define the landscape include Tall Shrub, Hummock, Semi-Wet, Wet and Tall Graminoid, as developed from Malmer et al. (2005) (Table 1 and Fig. 2). The *Tall*

*Shrub* cover class is underlain with permafrost but mostly consists of dwarf shrubs and a bottom layer of *Eriophorum vaginatum*. A sizable portion of the mire consists of *Hummock* palsa cover type, which is characterized as drained elevated permafrost plateaus with diverse vegetation similar to the Tall Shrub cover, but lacking tall shrubs (Table 1 and Fig. 2). These permafrost palsas are elevated about 1 m above the wet vegetated cover types and as permafrost thaws the palsas collapse into wet vegetation (Torbick et al., 2012). *Semi-Wet* is a wetter cover type carpeted with *Sphagnum* species but no visible open water areas. The areas characterized as *Wet* contain open water areas with floating *Sphagnum* species. *Tall Graminoid* areas consist of mostly *Carex rostrata* and *Eriophorum angustifolium* with high water table depth. The landscape at Stordalen is also comprised of rock and open water areas with no plant cover.

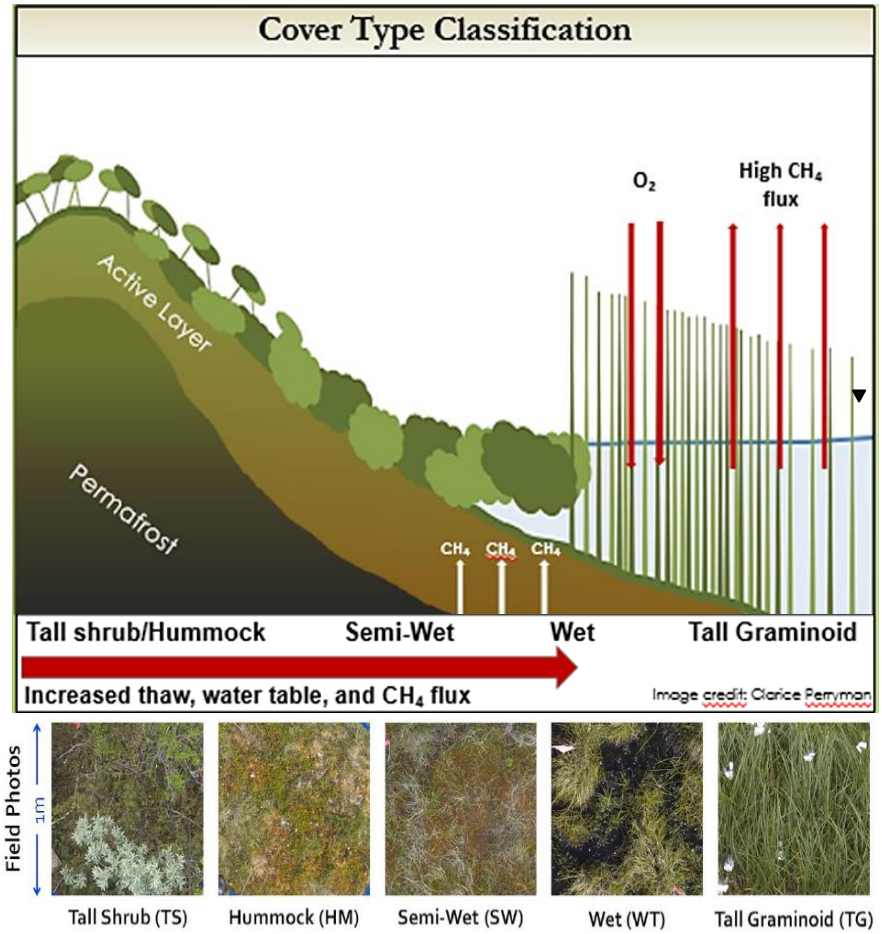


**Fig. 2.** The changes in vegetation cover type during permafrost degradation are represented as a sequence of increased thaw and deepening of the active layer (left to right). Fully thawed sites emit the greatest amount of $CH_4$. Additional land covers include open water, other, and rock. Image credit: Clarice Perryman and Christina Herrick

| **Table 1. Characteristic species composition for each vegetation cover type** | |
|---|---|
| Cover Type | Species Typical at Each Site |
| Tall Shrub (TS) | *Empetrum hermaphroditum, Betula nana, Rubus chamaemorus, Eriophorum vaginatum, Dicranum elongatum, Sphagnum fuscum, Cornus canadensis, Salix lapponum, Vaccinium uliginosum, Vaccinium vitisidaea.* |
| Hummock (HM) | *Empetrum hermaphroditum, Betula nana, Rubus chamaemorus, Eriophorum vaginatum, Dicranum elongatum, Sphagnum fuscum, Vaccinium uliginosum, Andromeda Polifolia.* |
| Semi-wet (SW) | *Eriophorum vaginatum, Carex rotundata, Sphagnum balticm,* other mosses. |
| Wet (WT) | *Eriophorum vaginatum, Carex rotundata, Sphagnum balticum,* other mosses. |
| Tall Graminoid (TG) | *Eriophorum angustifolium, Carex rostrata, Equisetum fluviatile* |
| Rock (RK) | Granite rock and stone pits |
| Open Water (H2O) | Water covered soil: lakes and ponds |
| Other | Built objects: Human structures, boardwalk, and buildings. |

### *2.4 UAS Image Data Collection*

Aerial imagery of Stordalen Mire (1 km x 0.5 km) was collected during the middle of the growing season using a fixed-wing unmanned aerial system with a mounted camera on July 11, 2014, July 11, 2015, July 12, 2016 and July 25, 2017. Poor weather conditions in July 2017, i.e. high wind, rain and cloud cover, resulted in flights taking place about two weeks later in July than previous years. However, vegetation cover does not vary greatly enough during this two-week time to result in error when comparing vegetation maps between years. The fixed-wing UAS was a Triton XL developed by Robota (www.robota.us), which is a small compact vehicle that allows for 0.5 kg of payload. The Robata Goose autopilot was used for automated flight line planning and flight tracking. The autopilot for the UAS allows for tracking of battery charge, airspeed, altitude, and other UAS mechanics during the flight. Flight lines were determined with

appropriate overlap between images to allow for image stitching based on designated flight speed and altitude.

Procedures for imagery collection were consistent for all four years (2014-2017). Favorable weather conditions were required for flight including low wind and minimal to no cloud cover. Flights began at 12:00 (UTC +1:00) when the sun is at the highest point in the sky which reduces shadows. The UAS was flown at an altitude of 70 meters and airspeed of 12 meters / second. During the flights, images were recorded every two seconds using an interval timer with up to 600+ images being captured during each 20-minute-long flight. Imagery was collected using a Panasonic Lumix-GM1 camera with three bands (red, green, and blue).

To capture the highest quality imagery, the fixed-wing UAS was flown several times during the month of July of each year. The best flights were determined through visual inspection of images, based on the number of clear and non-blurry images and light levels. Images were stitched together using Photoscan Pro 1.2 by AgiSoft (www.agisoft.com) to create a sub-centimeter photo mosaic. Photoscan was also used to also estimate the quality of each image through examination of image sharpness.

### *2.5 Georectification*

The fixed-wing UAS used did not contain a built-in GPS unit, therefore ground control points were needed to georeference the imagery. Ground control points were surveyed in 2015 using a Trimble GeoExplorer 6000 handheld GPS unit with an attached Trimble Tornado antenna. These points were collected along intersections of the boardwalk used to walk through the mire. The white boardwalk is easily distinguishable from the imagery and remained in a set location over the four years of data collection. Additional ground control points were collected at orange foam X's (1 m in length) placed across the mire, which are also easily recognizable

from the imagery. GPS coordinates were collected at the center of each X. These X's allowed for ground control points to be distributed across the mire as the boardwalk is concentrated around the edges of the area of interest. All ground control points were corrected for positional accuracy using SWEPOS® RINEX navigation files collected from a GNSS base station less than 2km away (Lantmäteriet, 2014). The corrected ground control points were then used within ArcGIS to georectify the image using a second order polynomial transformation.

### *2.6 Vegetation Plot Data Collection*

Vegetation plots were collected across Stordalen Mire and used as training data to classify the UAS imagery by cover type. In July 2015, randomized square-meter plots were measured for vegetation composition across the mire and individually classified into one of the five cover types (Fig. 2), each representing a different stage of permafrost degradation. Each plot was classified as one of the five cover types based on vegetation composition (Table 1) and the hydrological state, as previously described.

One hundred random points distributed across the mire were generated in ArcMap (Fig. 3) and used as the locations for plot measurements to remove any bias in location choice. The random points were uploaded into the Trimble GPS unit to navigate to the points in the field. It was not feasible to collect data at all one hundred points, due to time and weather, therefore, plot data was collected at the first seventy-five

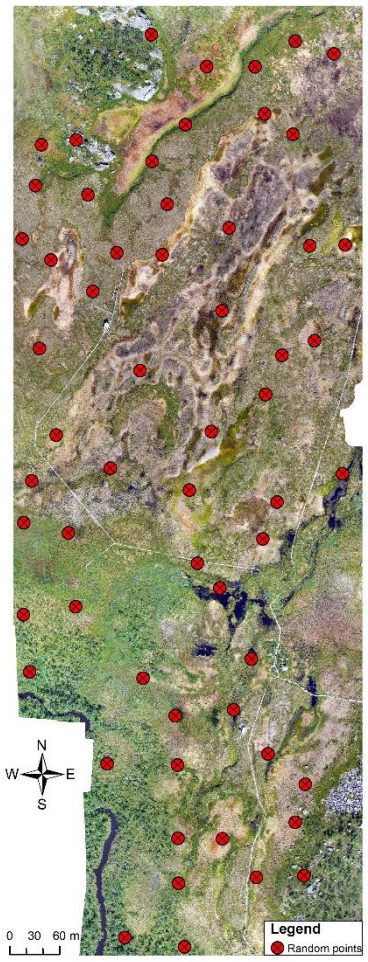


**Fig. 3.** 2014 UAS Imagery of Stordalen Mire (1 km x 0.5 km) overlaid with 100 random points used for vegetation plot locations.

random points. At each plot, GPS coordinates were collected at all four corners. Each plot was situated in a way that it contained only a single cover type and did not consist of a mix of two cover types (i.e. not on the edge of one cover type transiting into another).

### *2.7 UAS Image Classification*

Vegetation plots classified by cover type during the 2015 field season were used as training data to classify all four years of imagery. Plots collected in 2015 were individually inspected in ArcMap on the 2014, 2016 and 2017 UAS imagery to identify any difference in plot classification as the landscape changed. Any plots that appeared to have transitioned to a different cover type were removed from the classification. Also, if there was any uncertainty about whether a plot had maintained a cover class or not, then it was removed from the classification for that year (Fig. 4**)**. Additional cover type plots were added to the training data which included rock, open water, and other (boardwalk and stations at the mire).

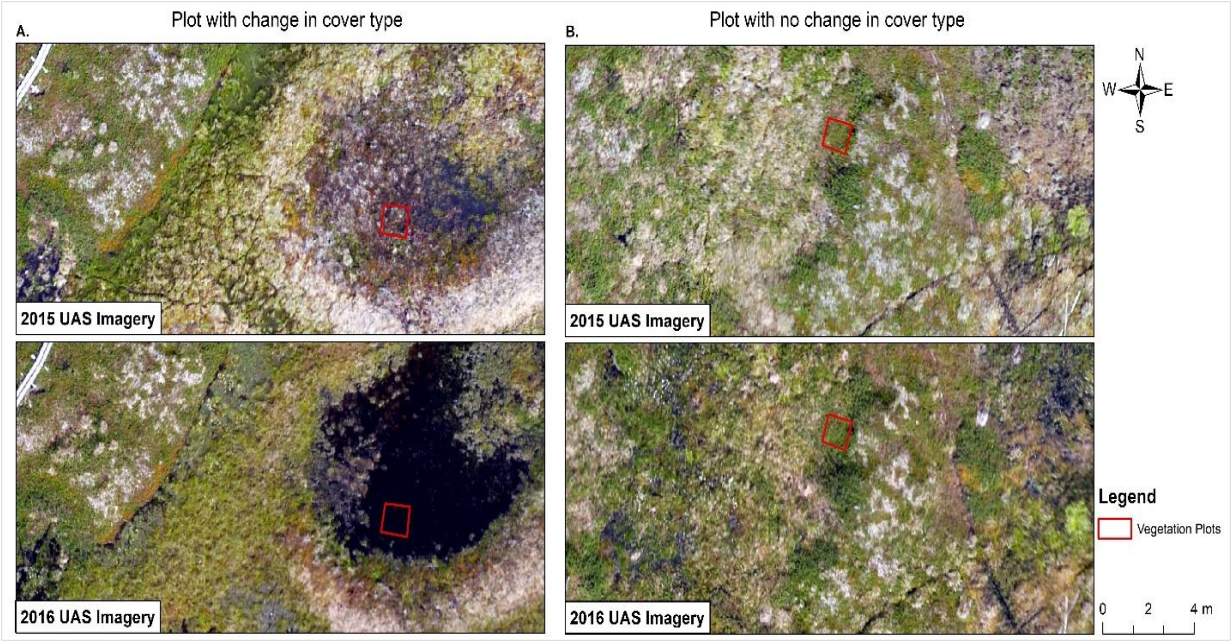


**Fig. 4.** Panel A and B show examples of the manual vegetation plot analysis. Vegetation plots were collected in 2015 classified in the field. Before these plots could be used to classify the 2014, 2016 and 2017 imagery they were individually inspected on each UAS image to determine if the cover type classification remained the same or not. Panel A shows a plot that transitioned from a semi-wet cover in 2015 to an open water cover type in 2016 and was therefore removed from the 2016 training data. Panel B shows a plot that maintained the hummock cover type from 2015 to 2016.

Code was developed in Google Earth Engine to classify the years of imagery using a Random Forest (RF) Classifier. The RF Classifier creates sets of Classification and Regression Trees (CARTs) to make a prediction based on a randomly selected subset of the training set (Belgiu and Drăguţ, 2016). Each classification tree is split based on this random subset. The final classification is determined by averaging the multiple tree class assignments (Fig. 5) (Breiman, 2001). For this study, 500 decision trees were generated. When using the RF Classifier, this is a commonly used value as errors stabilize before these 500 trees are reached (Belgiu and Drăguţ, 2016). Code was also developed to extract textural information from the imagery, which provides additional spatial context information and improves classification accuracy (Khatami et al. 2016). Textural analyses were only run on the green band due to the correlation between the red and blue spectral bands with the green band. We calculated minimum, maximum, mean, and

standard deviation as a 0.5 m x 0.5 m kernel. This kernel size was chosen as it is equivalent in size to the square meter quadrat used for the vegetation sampling. Also, entropy and angular secondary momentum were derived from a 3 x 3 co-occurrence matrix and added to the classification. Entropy measures the disorder of an image and is largest in areas where the image is not texturally uniform (Soares et al., 1997; Ouma et al., 2008). Angular secondary momentum or energy is inversely related to entropy and is a measure of textural uniformity (Ouma et al., 2008).

The outputs from the RF classifier were classification maps based on cover type for all four years of UAS imagery. From these classification maps, histograms were produced in Google Earth Engine based on the number of pixels in each cover class across the imagery. In Excel, these histograms were used to calculate the percent cover in each class based on the total number of pixels in each image. This data was then compared between years to see how the landscape changed over time.

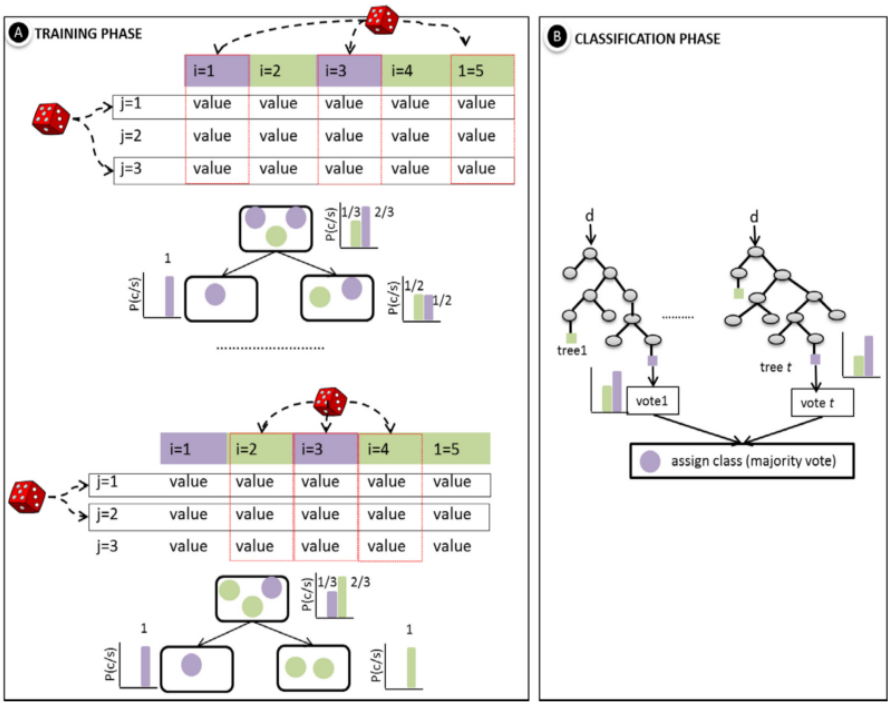


**Fig. 5.** Training and classification phases of Random Forest classifier. *i* = samples, *j* = variables, *p* = probability, *c* = class, s = data, *t* = number of trees, *d* = new data to be classified, and value = the different values that the variable *j* can have. Adapted from "Random forest in remote sensing: A review of applications and future directions," by M. Belgiu and L. Drăguţ, 2016, *ISPRS Journal of Photogrammetry and Remote Sensing, 114*(26). Copyright 2016 by ISPRS Journal of Photogrammetry and Remote Sensing

Validation data was used to analyze how well the classification performed, thus resulting in an overall classification accuracy value for each year of imagery. Twenty five percent of the training data was held back from the classification and used for validation. The remaining seventy five percent of the training data was used to classify the imagery. Error matrices were also developed in Google Earth Engine for each UAS classification. These matrices show how well each cover type was classified as well as which cover types may have been misclassified.

We coarsened the UAS classification images from 3 cm spatial resolution to 12 cm resolution to reduce some noise in the classification and any speckling that may occur. 3 cm pixels are very high resolution and may be too high to accurately define the individual pixels by cover type. We are mostly concerned with the dominant cover class and 12 cm may better fully capture individual species characteristic of a cover type. This scale was chosen as the square meter quadrat used for vegetation sampling was sub divided in 64 squares, each representing a 12.5 x 12.5 cm area. These individual squares were used to assess species composition characteristic of the cover types and fully captured individual species. The 12 cm scale was chosen to ensure that the imagery was coarsened by full pixels and not half pixels, which would had been the case if 12.5 cm was used. To coarsen the classified imagery, a focal mode sliding window function was used with a 12 cm kernel.

### *2.8 Estimating Land Cover Change via Classification Maps*

Vegetation cover was used as a proxy for estimating permafrost dynamics based on these cover type classification maps. The vegetation cover types were grouped into two categories, permafrost and non-permafrost, based on the thaw stages (Table 2). In Google Earth Engine, three types of maps were developed representing permafrost areas, non-permafrost areas (i.e. thawed sites) and other (rock and other). These maps were developed for the 2014 UAS imagery

classification and the 2017 UAS imagery classification to assess permafrost loss over the four-year period. The 2014 and 2017 permafrost and non-permafrost maps were compared on a per pixel basis. From this comparison, we were able to estimate the percent of the landscape where permafrost was lost, permafrost did not change, thawed areas that did not change and permafrost that was gained. For example, if a pixel was classified as permafrost in 2014, but was then classified as non-permafrost in 2017, then that pixel was determined to be a permafrost loss area. Permafrost gain is an unlikely scenario based on warming trends, however it is included in the analysis to assess the accuracy of the image classification.

**Table 2**: Cover Type Groupings Based on Permafrost Thaw Stage

| ***Cover Type Groupings*** | ***Cover Types*** |
|---|---|
| Permafrost | Tall Shrub and Hummock |
| Non-permafrost | Semi-wet, Wet, Open Water, and Tall Graminoid |
| Other | Other and Rock |

# 3. RESULTS

To characterize changes in vegetation distribution at Stordalen Mire, Abisko, Sweden we combined field-based measurements of species composition with four years of high resolution Unmanned Aerial System (UAS) imagery. These image classifications were compared to one another to analyze how the landscape changed each year from 2014-2017. Grouping the vegetation cover types based on intact permafrost or thaw we were able to estimate how permafrost dynamics changed over the study period.

## *3.1 UAS Imagery Data Collection*

The number of images collected and used for image stitching varied slightly between flights. For the 2014 UAS imagery, 457 images were collected, 411 images were stitched, and 161,125 tie points were used to create the mosaic. For the 2015 UAS imagery, 457 images were collected, 411 images were stitched, and 158718 tie points were used to create the mosaic. For the 2016 UAS imagery, 769 images were collected, 736 images were stitched, and 44,120 tie points were used to create the mosaic. Finally, for the 2017 UAS imagery, 589 images were collected, 559 images were stitched, and 1,213,608 tie points were used to create the mosaic. Differences in the total number of images collected varied due to minor differences in the flight plan used each year. We used medium to high settings for all Agisoft parameters for the stitching of photos. These included parameters to align photos, build dense point cloud, build mesh, build texture, and build orthromosaic. Different outputs on the number of photos aligned, tie points, and dense point cloud were a result of some images having more overlap or were more easily determined to have tie points. These differences did not alter the overall stitching

of the orthomosaic image. Images collected that were blurry were not used for stitching. The final mosaicked UAS images were represented by 7608 by 20736 pixels. After georectification the final resolution of the images was 3 cm. Corrected GPS positions had a horizontal dilution of precision (HDOP) less than equal to 2 and RMSE errors between 0.36-1.40 cm (mean = 0.63 cm, standard deviation = 0.21cm).

### *3.2 UAS Image Classifications*

The total number of vegetation plots used to classify the UAS imagery differed slightly between years. Plots collected in 2015 were individually inspected on the 2014, 2016 and 2017 UAS imagery to identify any difference in plot classification as the landscape changed. Any plots that appeared to have transitioned to a different cover type were removed from the classification. Also, if there was any uncertainty about whether a plot had maintained a cover class or not, then it was removed from the classification for that year (Fig. 4). After individually inspecting the 2015 plots on each year of UAS imagery, the final number of plots

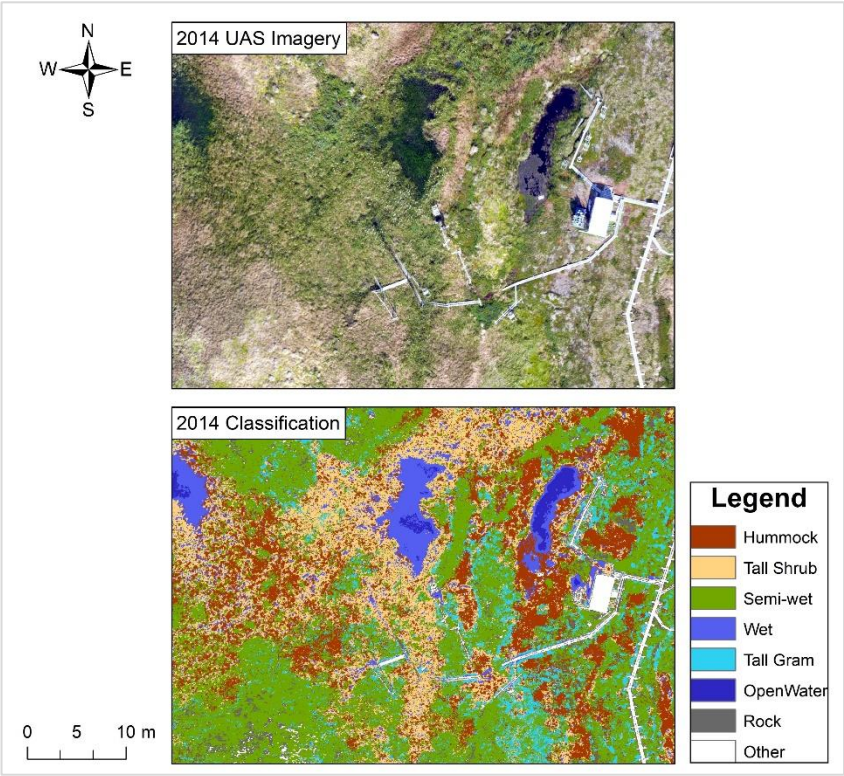


**Fig. 6.** This panel is displaying a zoomed in portion of the 2014 UAS imagery RGB (top) from Stordalen Mire and the 2014 UAS imagery classified by cover type (bottom). The white path seen in the imagery is the boardwalk used to walk through the mire and is connected to the white equipment shack.

used to train the classifications included 89 plots for 2014, 94 for 2015, 84 for 2016 and 81 for 2017. Rock, Other and Open Water plots were added to the training data through manual interpretation from the UAS imagery.

Using a Random Forest Classifier, each year of UAS imagery was classified by cover type and compared to one another to assess changes in vegetation. The output of this analysis included a classification map for each year of UAS imagery, which characterized the entire area of Stordalen Mire by the eight defined cover types (Fig. 6). Speckling across these maps were reduced by coarsening the classification from 3 cm to 12 cm spatial resolution (Fig. 7). From these classification maps, the percent cover was quantified for each cover type and compared between years (Fig. 8). The hummock cover type, representing intact permafrost areas, decreased coverage over the four-year period. Hummock coverage was highest in 2014 and 2015 at 33% and lowest in 2017 at 24%. Tall shrub coverage varied over the study period but was significantly higher in 2014 compared to the following years. The Semi-wet cover type (i.e. collapsed hummock palsas) increased coverage by 18% from, 2014 to 2017. Percent coverage of the Wet cover type varied over the study period with a low of 2% in 2015 and highs in 2016 and 2017 at 15%. The Tall graminoid cover type, representing fully thawed areas, decreased coverage by 8.5% from 2014 to 2017. Open water also varied over the study period with 2015 having the highest percent cover at 11%. Percent coverage of the Rock cover type varied with the highest percentage coverage in 2017 at 7% and the lowest in 2016 at 1%. There were small variations in the percent cover of the Other class over the four years as values remained at about 1%. Hummock was the dominant cover type in 2014, while semi-wet was the dominate cover type in 2015, 2016 and 2017.

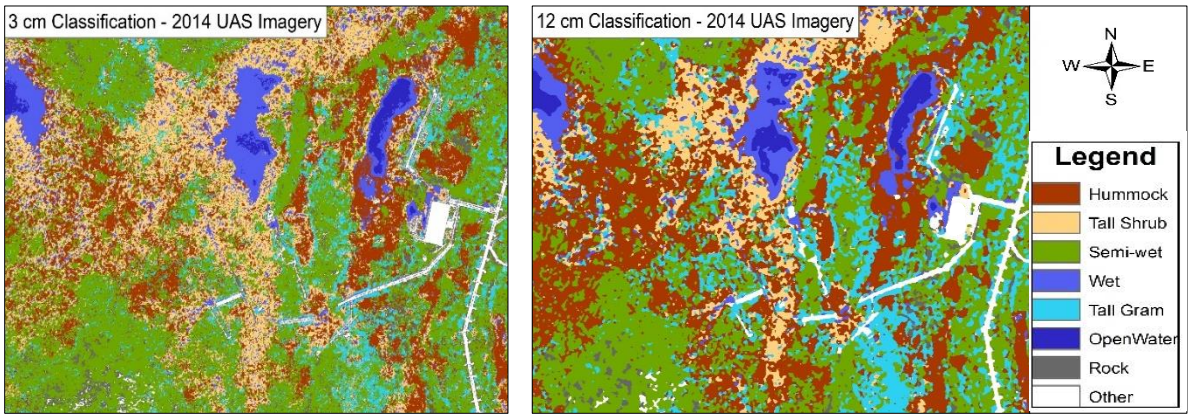


**Fig. 7.** This panel is comparing the 3 cm spatial resolution classified 2014 Stordalen Mire UAS imagery at (left) to the 12 cm spatial resolution classification (right). These images represent a zoomed in portion of Stordalen Mire.

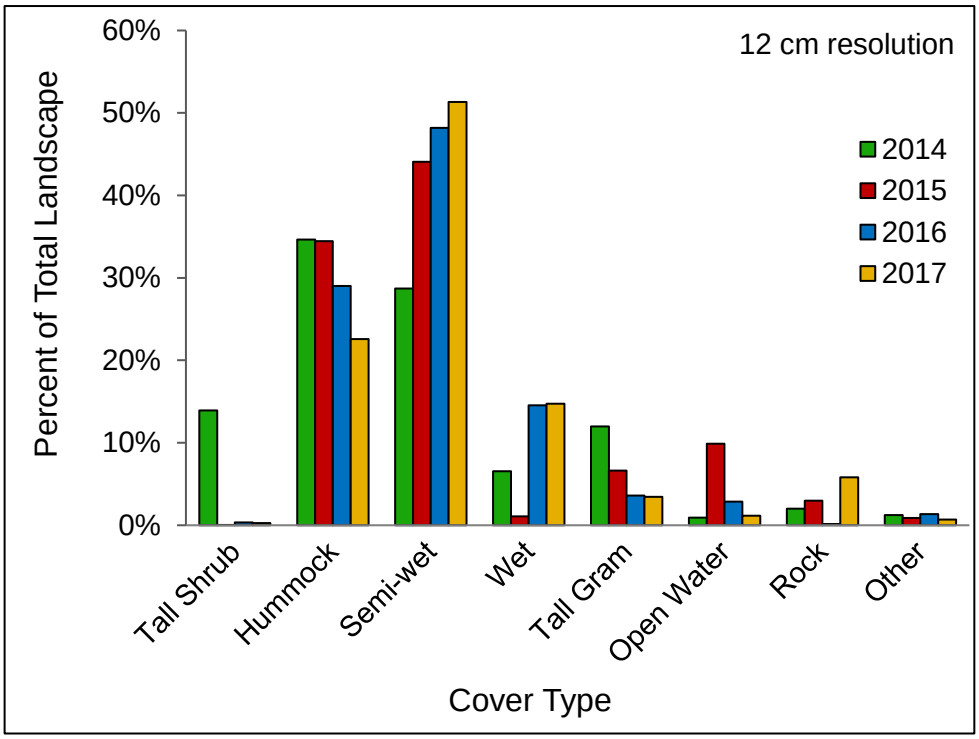


**Fig. 8.** Percent coverage across Stordalen Mire of each cover type for the years 2014, 2015, 2016 and 2017. HM = Hummock; TS = Tall Shrub; SW = Semi-wet; TG = Tall Graminoid; H20 = Open Water.

### *3.3 Error analysis and cover class assessment*

Validation error for each UAS imagery was calculated in Google Earth Engine to provide insight into how well the Random Forest (RF) Classifier performed in assigning classes. From this, overall classification accuracy was calculated for each cover type map. The overall classification accuracy for 2014-2017 was 80.6%, 79.1%, 82.0%, and 82.9%, respectively. We also calculated error matrices to visually analyze the performance of the RF Classifier on each UAS imagery (Table 3). These matrices show how well the RF Classifier assigned classes as well as any misclassifications. The error matrix for the 2014 classification revealed that hummock was misclassified as wet and tall shrub, while tall shrub was misclassified as hummock and tall graminoid. The semi-wet cover type was often misclassified as hummock. For the 2015 classification, hummock was often misclassified as semi-wet, while semi-wet was misclassified as hummock and tall graminoid. Tall shrub and tall graminoid cover classes were often misclassified as one another. In 2016, the cover types tall shrub, semi-wet, and tall graminoid were misclassified as hummock. Hummock and tall shrub were misclassified as semi-wet, while hummock was also often misclassified as rock. Finally, the 2017 classification error matrix revealed that semi-wet and tall graminoid were misclassified as hummock, while hummock was misclassified as semi-wet and tall shrub. For all four classifications, the cover classes open water, rock and other were well classified.

**Table 3: UAS Imagery Classification Error Matrices 2014 - 2017**

HM = Hummock, TS = Tall shrub, SW = Semi-wet, TG = Tall Graminoid, H20 = Open Water, RK = Rock, and OT = Other

2014 UAS Imagery Classification Error Matrix

| | | *Reference Data* | | | | | | | |
|---|---|---|---|---|---|---|---|---|---|
| | | **HM** | **TS** | **SW** | **WT** | **TG** | **H20** | **RK** | **OT** |
| *Classified Data* | **HM** | 61 | 4 | 0 | 13 | 1 | 0 | 0 | 0 |
| | **TS** | 5 | 18 | 2 | 0 | 6 | 0 | 0 | 0 |
| | **SW** | 7 | 1 | 60 | 0 | 3 | 0 | 0 | 0 |
| | **WT** | 0 | 0 | 0 | 14 | 0 | 4 | 0 | 0 |
| | **TG** | 4 | 0 | 4 | 0 | 32 | 0 | 0 | 0 |
| | **H20** | 0 | 0 | 0 | 0 | 0 | 22 | 0 | 0 |
| | **RK** | 2 | 0 | 1 | 0 | 0 | 0 | 21 | 0 |
| | **OT** | 0 | 0 | 0 | 0 | 0 | 0 | 0 | 9 |

2015 UAS Imagery Classification Error Matrix

| | | *Reference Data* | | | | | | | |
|---|---|---|---|---|---|---|---|---|---|
| | | **HM** | **TS** | **SW** | **WT** | **TG** | **H20** | **RK** | **OT** |
| *Classified Data* | **HM** | 45 | 6 | 11 | 0 | 8 | 0 | 0 | 0 |
| | **TS** | 2 | 28 | 0 | 0 | 4 | 0 | 0 | 0 |
| | **SW** | 4 | 3 | 66 | 0 | 4 | 0 | 0 | 0 |
| | **WT** | 2 | 0 | 0 | 19 | 0 | 3 | 0 | 0 |
| | **TG** | 3 | 5 | 3 | 0 | 28 | 0 | 0 | 0 |
| | **H20** | 4 | 0 | 0 | 0 | 0 | 19 | 0 | 0 |
| | **RK** | 0 | 0 | 0 | 0 | 0 | 0 | 24 | 0 |
| | **OT** | 0 | 0 | 0 | 0 | 0 | 0 | 0 | 7 |

2016 UAS Imagery Classification Error Matrix

| | | *Reference Data* | | | | | | | |
|---|---|---|---|---|---|---|---|---|---|
| | | **HM** | **TS** | **SW** | **WT** | **TG** | **H20** | **RK** | **OT** |
| *Classified Data* | **HM** | 68 | 0 | 5 | 0 | 0 | 0 | 5 | 0 |
| | **TS** | 3 | 31 | 3 | 0 | 0 | 0 | 0 | 0 |
| | **SW** | 4 | 0 | 44 | 1 | 3 | 0 | 2 | 0 |
| | **WT** | 0 | 0 | 0 | 18 | 0 | 0 | 0 | 0 |
| | **TG** | 9 | 3 | 5 | 2 | 10 | 0 | 0 | 0 |
| | **H20** | 0 | 0 | 0 | 0 | 0 | 17 | 0 | 0 |
| | **RK** | 0 | 0 | 0 | 0 | 0 | 0 | 11 | 0 |
| | **OT** | 0 | 0 | 0 | 0 | 0 | 0 | 0 | 6 |

2017 UAS Imagery Classification Error Matrix

| | | *Reference Data* | | | | | | | |
|---|---|---|---|---|---|---|---|---|---|
| | | **HM** | **TS** | **SW** | **WT** | **TG** | **H20** | **RK** | **OT** |
| *Classified Data* | **HM** | 26 | 2 | 3 | 0 | 1 | 0 | 0 | 0 |
| | **TS** | 0 | 21 | 0 | 0 | 0 | 0 | 0 | 0 |
| | **SW** | 16 | 0 | 33 | 2 | 7 | 0 | 0 | 0 |
| | **WT** | 0 | 0 | 0 | 19 | 0 | 1 | 0 | 0 |
| | **TG** | 6 | 0 | 3 | 0 | 40 | 0 | 0 | 0 |
| | **H20** | 0 | 0 | 0 | 0 | 0 | 26 | 0 | 0 |
| | **RK** | 0 | 0 | 0 | 0 | 0 | 0 | 28 | 0 |
| | **OT** | 0 | 0 | 0 | 0 | 0 | 0 | 0 | 6 |

### *3.5 Quantification of Land Cover Change*

Vegetation cover determined from the 3 cm resolution classification maps was used to estimate permafrost dynamics across the landscape over time. The amount of permafrost was quantified in the 2014 and 2017 imagery by grouping cover types underlain with permafrost.

From this grouping and comparison of the 2014 to 2017 UAS classification, we determined the percent of Stordalen Mire that (1) remained permafrost (2) transitioned from permafrost to thaw (3) remained thawed (4) gained permafrost. These results show that over the four-year period 20% of the landscape thawed, 5% of the area remained intact permafrost, 66% of the area remained thawed, and 6% of the area increased in permafrost (Table 4).

**Table 4: Estimation of Permafrost Dynamics 2014 – 2017**
Vegetation cover types were grouped by thaw stage and used as a proxy to estimate changes in permafrost based on the 2014 and 2017 UAS imagery classification maps.

| | Percent of Total Landscape |
|---|---|
| *Permafrost Loss* | 20.0% |
| *Permafrost No Change* | 5.2% |
| *Thaw No Change* | 66.3% |
| *Permafrost Gain* | 6.2% |

### *3.6 Temperature and Precipitation Trends*

Temperature and precipitation data was collected at Stordalen Mire throughout the study period (2014-2017) to see how climate variability may have impacted vegetation distribution. The temperature data was collected in ten-minute intervals and averaged monthly for each year (Fig. 9). Due to instrumentation error, no values of temperature or precipitation are reported for January 2014. Average monthly temperature was greatest during the month of July for each year, except in 2015 where August had the highest value. December was the coldest month on average in 2014, however this may not be an accurate conclusion as data is missing for January of that year. Average temperature was lowest in January for 2015 and 2016, while February was the coldest month on average in 2017. There is no consistent trend in increasing temperature over time. As mentioned, the UAS imagery was collected during July of each year. 2014 had a

significantly higher July average temperature compared to the following years. Monthly total precipitation was also collected at Stordalen Mire and compared between years (Fig. 10). For each year, July had the greatest total monthly precipitation, with 2016 having the greatest total and the lowest in 2014 during that month. Precipitation and temperature was greatest during June to September and lowest during December to March.

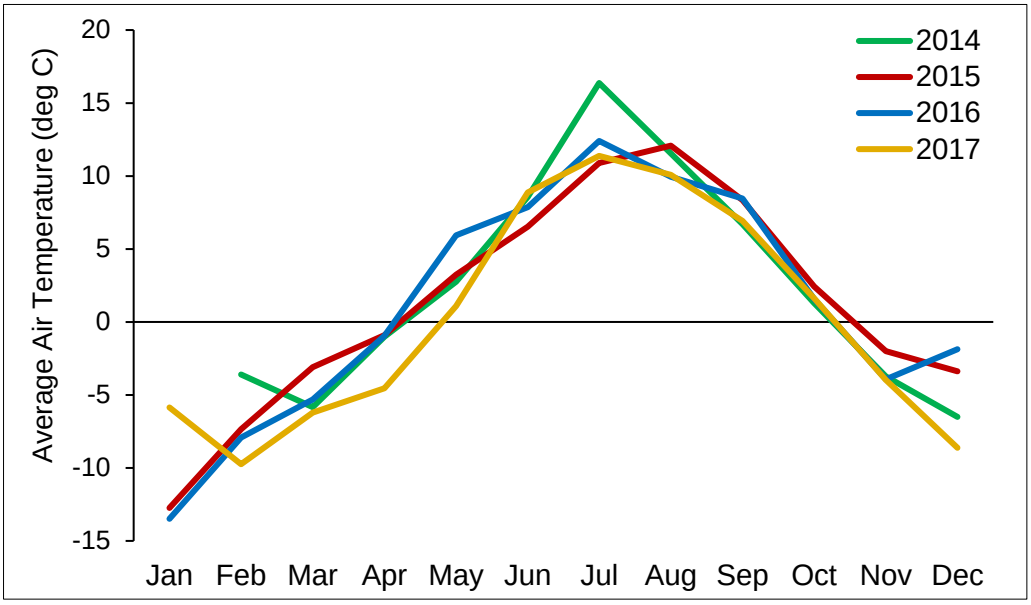


**Fig. 9:** Monthly average air temperature in degrees Celsius for the years 2014-2017 from the ICOS Sweden station Abisko-Stordalen.

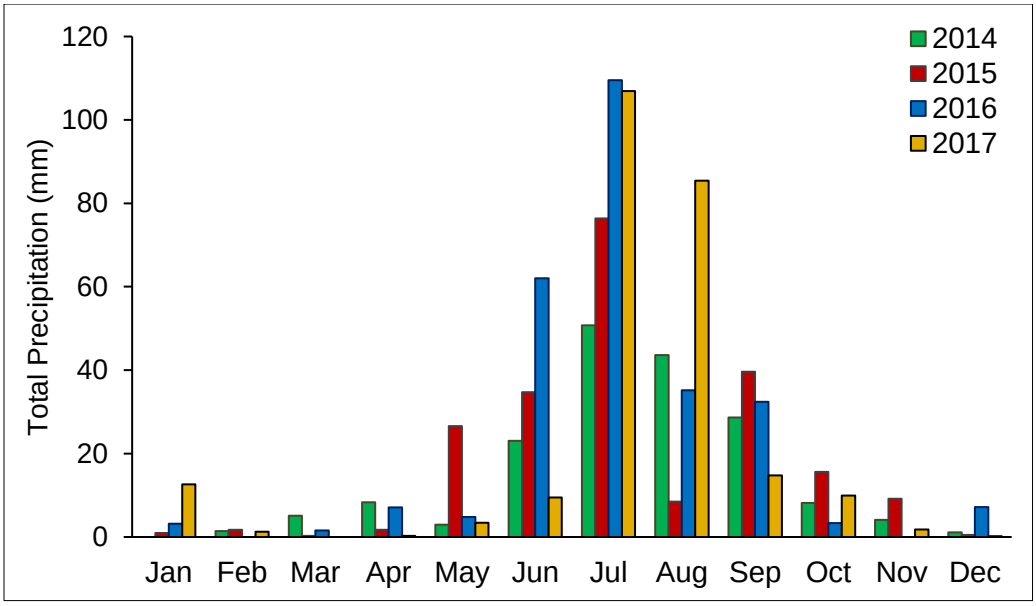


**Fig. 10:** Monthly total precipitation for the years 2014-2017 from the ICOS Sweden station Abisko-Stordalen.

# 4. DISCUSSION

Four years of high resolution UAS imagery collected at Stordalen Mire allowed us to capture the complex spatial heterogeneity of the vegetation and assess vegetation changes in response to permafrost thaw. Ground level vegetation observations provide insight into plot scale thaw processes; however, they do not capture patterns of thaw across the landscape. Our methodology of collecting UAS imagery provides a low cost, repeatable method for studying the highly heterogenous northern peatland ecosystems. We combined field measurements of vegetation cover with the UAS imagery to classify study area by cover type using a Random Forest Classifier. These four cover type maps were compared to one another to analyze how the landscape changed from 2014-2017. These results indicate a rapid response to permafrost thaw. It was advantageous to group the vegetation into cover type classes to assess how the vegetation has changed at various stages of permafrost degradation.

## *4.1 UAS Image Processing and Classification*

To accurately georectify the UAS imagery, the collection of high precision GPS points were crucial. Our methodology of placing and pinning down large foam X's throughout the mire prior to flight allowed for control points to be distributed evenly across the study area. These X's were inexpensive, easily visible from the imagery and were not destructive to the mire. After the imagery was georectified, the final spatial resolution was 3 cm. This high resolution captured small variations across the landscape, which was crucial for accurately classifying the heterogenous cover types.

Google Earth Engine allowed us to perform several operations on the UAS imagery including extracting textural information, classifying the imagery, running statistical analyses, and obtaining validation accuracies and error matrices. Therefore, it was advantageous using a single platform for various steps involved in image processing. The processing speed using Google Earth Engine was much greater than previous attempts. Textural analysis and an artificial neural network (ANN) classification was run on the 2014 UAS imagery in Python (v. 2.7) using Intel(R) Xeon(R) CPU 2.67GHz with 4 CPU Cores with 24 GB RAM. The textural analysis, including entropy, angular secondary moment, evenness, standard deviation, minimum, maximum, and range, took 72 hours to run. Coding the ANN took 24 hours to run and then another 12 hours to determine the classification error (M. Palace, personal communication, May 15, 2018). Textural analysis, the random forest classification, and error analysis each only needed several minutes to run using Google Earth Engine.

The Random Forest Classifier performed well classifying the years of UAS imagery as accuracies ranged between 79.1% and 82.9%. The high accuracy in this study is most likely due to the robust training data and higher spatial resolution of the imagery. Training data was especially useful for the cover types with variable species composition and water table depths, which may have been difficult to differentiate from the imagery alone.

### *4.2 Vegetation Changes*

Using the four years of UAS classified imagery, we were able to assess differences in cover types across the landscape over time. The hummock cover type, representing intact permafrost areas, decreased coverage over the four-year period. Hummock coverage was highest in 2014 and 2015 at about 33% and lowest in 2017 at 24% (Fig. 8). Hummock class was mostly confused as Rock due to the spectral similarities of lichen in the hummock areas and that of

rocks. These hummock areas represent elevated palsa mounds underlain with permafrost. As permafrost thaws, these palsas collapse and the vegetation transitions into a sphagnum dominated composition represented as the semi-wet cover type. This decrease in the hummock cover type and increase in semi-wet over the four-year study period is an indication of permafrost collapse.

Tall shrub coverage varied over the study period but was significantly higher in 2014 compared to the following years. Decreases in tall shrub and hummock areas are consistent with the findings of Malmer et al. (2005), which compared vegetation maps of Stordalen Mire from 1970 and 2000. A reduction in tall shrubs in these ecosystems can promote thaw as the lack of tall shrubs allows more solar radiation to reach the surface, thus increasing surface temperatures (Quinton et al., 2009; Chasmer et al., 2011). There is however, uncertainty associated with the interpretation of this class. The error matrices revealed that the tall shrub class was often misclassified as tall graminoid, similar to previous classification efforts (M. Palace, personal communication, May 15, 2018). The UAS imagery does not include the landscape topography, therefore plant heights were not used to differentiate classes. The tall shrub and tall graminoid classes differ in plant height and elevation as the tall shrubs are underlain with permafrost. Topographical analyses thus may aid in the separation of the tall shrub and tall graminoid class. Also, *Betula nana*, the dominate species in the tall shrub class, grows as tall as 5 -7 feet at Stordalen Mire, therefore it was not practicable to place the quadrats over these taller shrubs. This class may have been better differentiated if training data was collected at these taller stands.

Percent coverage of the thawed vegetation cover types varied over the four-year study period, but overall the landscape is becoming wetter (Fig. 11). The Semi-wet cover type (i.e. collapsed hummock palsas) increased coverage by 18% from 2014 to 2017 (Fig. 8). This cover

type represents collapsed hummock areas, therefore this increase over the study period makes sense as hummock decreased. Percent coverage of the Wet cover type varied over the study period with a low of 2% in 2015 and highs in 2016 and 2017 at 15% (Fig. 8). This wetter landscape in 2016 and 2017 (Fig. 8) can be seen to correlate with the high July precipitation during those years (Fig. 10). We may also be seeing a lag effect from the warm, dry summer of 2014, which are conditions that promote permafrost thaw. Hummock was the dominant cover type in 2014, while Semi-wet was the dominate cover type in 2015, 2016 and 2017. Open water also varied over the study period with 2015 having the highest percent cover at 11% (Fig. 8). These variations may be a result of vegetation such as sphagnum growing in and around the open water areas. In 2015, Wet coverage was significantly lower than the other years, while the open water coverage in 2015 was significantly higher than other years. This may be a result of open water and wet sites being missed classified with open water being over classified.

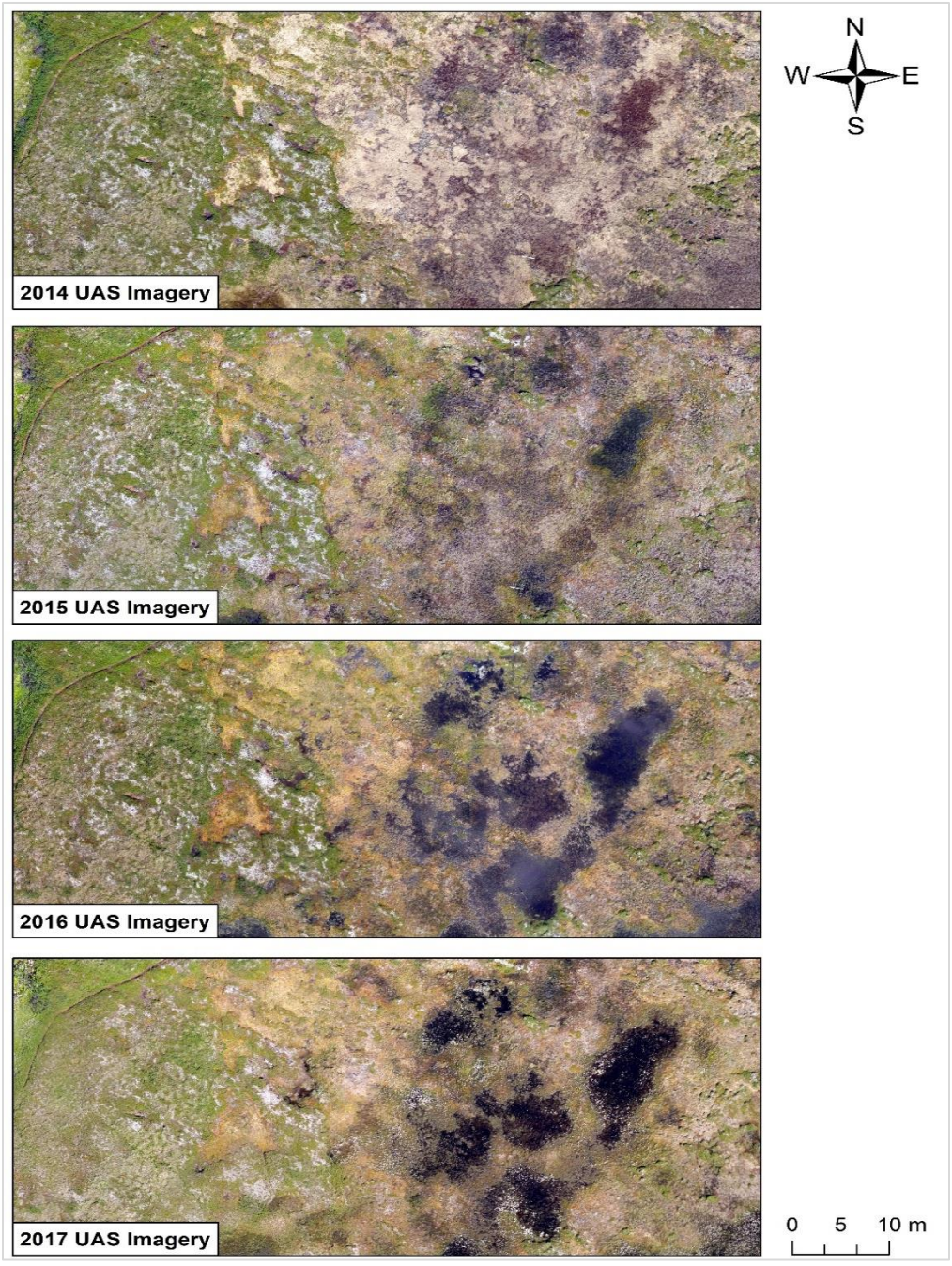


**Fig. 11.** This panel shows a four-year comparison of the same zoomed in portion of the mire as a visual representation of how wetness has increased over time. The darker areas indicate a wetter landscape.

The Tall graminoid cover type, representing fully thawed areas, decreased coverage by 8.5% from 2014 to 2017 (Fig. 7). This is contradictory to previous studies which found an increase in the tall graminoid cover class due to the landscape becoming wetter with thaw (Malmer et al., 2005). The tall graminoid areas do not necessarily represent areas that were once

intact permafrost. For the tall graminoid vegetation to develop, there must be flowing water and nutrients through the fen area. At Stordalen Mire, the tall graminoid cover class is clustered in a fen area where water drains through the fen into the northern lake Inre Harrsjön. In each classification map, tall graminoid was often misclassified as another cover type. There could be several reasons for these misclassifications. The tall graminoid vegetation consists of tall sedges, which shift easily with the breeze. Therefore, this area of the mire dominated by the tall graminoid cover type tends to have the most blur in the UAS images. These tall sedges may also cast shadows on surrounding sedges, resulting in misclassification of those shadowed pixels. Another probable reason for the error in tall graminoid is due to the higher water table, characteristic of the cover type. This water table may be visible from the imagery, thus causing these areas to be classified as Wet or Open water.

The Rock and Other cover classes represent the smallest portion of the landscape, but also varied slightly over the four years (Fig. 7). The small variations in Rock cover between the years may be due to changes in vegetation growing on these rocks. Also, shadow angle differed slightly between flights possibly due to slight differences in the timing of flights. Since the rocks vary in elevation across the landscape, different areas of a rock may have been shadowed and therefore misclassified. Percent cover of the Other class over the four years remained at about 1% (Fig. 7). Small variations are most likely due to the boardwalk sinking as water table increases and the tall sedges growing over the boardwalk. Also, in 2016 construction on the boardwalk took place which increased its area.

Permafrost thaw and subsequent vegetation changes are a result of changes in climate including increases in temperature and precipitation (Van Der Kolk et al., 2016). Temperature and precipitation trends over the past several decades, rather than only four years, may provide a

better insight into how the climate has been changing. The results presented in this study may be a resulting lag effect from years of increases in temperature and precipitation. During the last two decades, the Abisko area has experienced deeper snow cover and increased winter precipitation (Kohler et al., 2006). This can contribute to permafrost degradation as deeper snow cover acts as insulation, keeping the ground warmer and thus preventing colder temperatures to reach lower peat depths (Johannsson et al., 2006).

Increases in summer precipitation can also impact the hydrological regime of the landscape, further promoting permafrost thaw. Increases in snow cover results in increased water inputs to the system in the form of melt water (Quinton et al., 2009). Permafrost plateaus (hummocky palsa mounds) serve as runoff sources as their thin active layer cannot absorb all water inputs. Additional water inputs are therefore drained to the surrounding fen areas resulting in increased landscape connectivity as the water table level increases (Bowling et al., 2003; Quinton et al., 2009; Quinton et al., 2011). Increased water levels strongly impact the rate of permafrost thaw, which is influenced by soil moisture. This is because wet peat, compared to dry peat, is a better conductor of energy from the ground surface to the frost table, thus promoting thaw (Quinton et al., 2009; Quinton et al., 2011). Therefore, a higher soil moisture content due to increased water inputs promotes permafrost degradation and results in changes to the vegetation (Torbick et al., 2012; Van Der Kolk et al., 2016; Quinton et al., 2009). To observe such changes at the landscape level, several more years of UAS imagery can be analyzed for changes in wetness. For a deeper understanding of drivers of vegetation changes, this imagery can be analyzed in conjunction with data on snow depth and water table levels across the landscape.

### *4.3 Implications on the Carbon Balance*

Vegetation changes as a result of permafrost thaw have implications on the physical environment and on the carbon balance. Several studies conducted at Stordalen Mire have linked vegetation changes over the past several decades to increases in carbon dioxide and methane emissions (Malmer et al., 2005; Bäckstrand et al., 2009; Christensen et al., 2004). The drier parts of the mire, associated with hummocky and tall shrub vegetation, have been shown to be significantly lower in $CH_4$ emissions compared to wetter sites (Jackowicz-Korczyński et al., 2010). Water table depth is another controlling factor of variations in $CH_4$, as $CH_4$ can be emitted through diffusion, ebullition or through vascular plants (Granberg et al., 1997). The results from this study indicate that the landscape is becoming wetter and vegetation underlain with permafrost is decreasing in dominance. Therefore, it would be beneficial to link the percent cover estimates from this study with measured methane flux rates from each cover type to better understand how the carbon balance at the mire is changing over time.

### *4.5 Estimation of Land Cover Change*

Using vegetation as a proxy, the classified 2014 and 2017 UAS imagery were compared to one another to estimate how permafrost dynamics have changed. These results show that over the four-year period 20% of the landscape thawed, 5% of the area remained intact permafrost, 66% of the area remained thawed, and 6% of the area increased in permafrost (Table 4). These results show how rapidly the landscape has changed over four years.

### *4.6 Future Work*

There are several areas of this study that can expanded upon for future work. The 2015 vegetation plots were also measured for species composition. Therefore, this data can be used in conjunction with the UAS imagery to estimate species composition across the landscape. A

benefit of using Unmanned Aerial Systems (UAS) imagery is the ability for it to be linked with coarser satellite imagery at higher spectral and spatial coverage. Scaling up may increase the error of the classification as species diversity may increase. However, the classification scheme used in this study defines classes that remain structurally similar even if the vegetation varies. Scaling to a larger region of the northern ecosystems would allow for a better understanding of how the landscape and carbon dynamics of the region are changing in response to permafrost thaw. As mentioned, differences in topography may aid in differentiating cover types as vegetation differs in height. Intact permafrost areas are elevated surfaces compared to the thawed fen areas where permafrost has collapsed. Studying topography using Lidar, for example, could provide insight into difference in water table level at the various cover types. Also, observing trends in snow cover and water table depths at Stordalen Mire may provide better insight into causes of vegetation changes. Finally, measured methane emission rates from each cover type can be linked with the classification maps to estimate changes in emissions across the landscape over time.

# 5. CONCLUSION

The spatial heterogeneity of Stordalen Mire was effectively captured through the collection of four years of high resolution spatial data using an Unmanned Aerial System (UAS). We combined field-based measurements of vegetation cover with four years of UAS imagery to examine vegetation changes in response to permafrost thaw. Using a fixed wing and automated flight plan allowed for a steady flight with consistent airspeed and height. High precision GPS data was needed to accurately georeference the aerial imagery. Google Earth Engine allowed for fast computations of several operations on the UAS imagery including extracting textural information, classifying the imagery, running statistical analyses, and obtaining validation accuracies and error matrices. The Random Forest Classifier was an effective tool for using the vegetation training to classify the UAS imageries. Grouping species into vegetation cover types provided a simplified classification scheme which can be scaled to coarser resolution imagery with a larger spatial coverage. Differences in percent cover of the vegetation types over the four years based on the UAS imageries revealed that the landscape is shifting towards wetter vegetation cover. Hummock cover type, representing intact permafrost areas, decreased coverage by 9%, while semi-wet cover, representing collapsed hummock, increased coverage by 18%. These results indicate a rapid response to permafrost thaw over the four-year period. This progression of thaw and increase in landscape wetness has impacts on the carbon balance as $CH_4$ emissions are greater at higher water table areas and wetter vegetation sites. Discontinuous permafrost regions are highly vulnerable to climate changes; therefore, it is crucial to understand ecosystem changes at the landscape level. The use of a UAS allowed us to effectively study vegetation changes across Stordalen Mire in response to permafrost thaw.

# 6. BIBLIOGRAPHY


Anderson, K., & Gaston, K. J. (2013). Lightweight unmanned aerial vehicles will revolutionize spatial ecology. *Frontiers in Ecology and the Environment*, *11*(3), 138–146. https://doi.org/10.1890/120150

Bäckstrand, K., Crill, P. M., Jackowicz-Korczyński, M., Mastepanov, M., Christensen, T. R., & Bastviken, D. (2009). Annual carbon gas budget for a subarctic peatland, northern Sweden. *Meddelanden Fran Lunds Universitets Geografiska Institutioner, Avhandlingar*. https://doi.org/10.5194/bgd-6-5705-2009

Belgiu, M., & Drăgu, L. (2016). Random forest in remote sensing: A review of applications and future directions. *ISPRS Journal of Photogrammetry and Remote Sensing*. https://doi.org/10.1016/j.isprsjprs.2016.01.011

Billings, W. D., Luken, J. O., Mortensen, D. A., & Peterson, K. M. (1982). Arctic tundra: A source or sink for atmospheric carbon dioxide in a changing environment? *Oecologia*, *53*(1), 7–11. https://doi.org/10.1007/BF00377129

Bowling, L. C., Kane, D. L., Gieck, R. E., Hinzman, L. D., & Lettenmaier, D. P. (2003). The role of surface storage in a low-gradient Arctic watershed. *Water Resources Research*, *39*(4). https://doi.org/10.1029/2002WR001466

Breiman, L. (2001). Random forests. *Machine Learning*, *45*(1), 5–32. https://doi.org/10.1023/A:1010933404324

Chasmer, L., Quinton, W., Hopkinson, C., Petrone, R., & Whittington, P. (2011). Vegetation Canopy and Radiation Controls on Permafrost Plateau Evolution within the Discontinuous Permafrost Zone, Northwest Territories, Canada. *Permafrost and Periglacial Processes*, *22*(3), 199–213. https://doi.org/10.1002/ppp.724

Christensen, T. R., Johansson, T., Jonas Å Kerman, H., Mastepanov, M., Malmer, N., Friborg, T., Svensson, B. H. (n.d.). Thawing sub‐arctic permafrost: Effects on vegetation and methane emissions. https://doi.org/10.1029/2003GL018680

Deng, J., Li, C., Frolking, S., Zhang, Y., Bäckstrand, K., & Crill, P. (2014). Assessing effects of permafrost thaw on C fluxes based on multiyear modeling across a permafrost thaw gradient at Stordalen, Sweden. *Biogeosciences*. https://doi.org/10.5194/bg-11-4753-2014

Franklin, S. E., & Wulder, M. A. (2002). Remote sensing methods in medium spatial resolution satellite data land cover classification of large areas. *Progress in Physical Geography*, *26*(2), 173–205. https://doi.org/10.1191/0309133302pp332ra

Gislason, P. O., Benediktsson, J. A., & Sveinsson, J. R. (2006). Random forests for land cover classification. In *Pattern Recognition Letters* (Vol. 27, pp. 294–300). https://doi.org/10.1016/j.patrec.2005.08.011

Granberg, G., Mikkelä, C., Sundh, I., Bo, H. S., & Nilsson, M. (1997). Sources of spatial variation in methane emission from mires in northern Sweden: A mechanistic approach in statistical modeling. *Global Biogeochemical Cycles*, *11*(2), 135–150.

Hugelius, G., Strauss, J., Zubrzycki, S., Harden, J. W., Schuur, E. A. G., Ping, C. L., … Kuhry, P. (2014). Estimated stocks of circumpolar permafrost carbon with quantified uncertainty ranges and identified data gaps. *Biogeosciences*, *11*(23), 6573–6593. https://doi.org/10.5194/bg-11-6573-2014

Jackowicz-Korczyński, M., Christensen, T. R., Bäckstrand, K., Crill, P., Friborg, T., Mastepanov, M., & Ström, L. (2010). Annual cycle of methane emission from a subarctic peatland. *Journal of Geophysical Research G: Biogeosciences*, *115*(2). https://doi.org/10.1029/2008JG000913

Johansson, T., Malmer, N., Crill, P. M., Friborg, T., Åkerman, J. H., Mastepanov, M., & Christensen, T. R. (2006). Decadal vegetation changes in a northern peatland, greenhouse gas fluxes and net radiative forcing. *Global Change Biology*. https://doi.org/10.1111/j.1365-2486.2006.01267.x

Kattsov VM, Källén E, Cattle H et al. (2005) Chapter 4: Future climate change: modeling and scenarios for the Arctic. In: *Arctic Climate Impact Assessment – Scientific Report* (eds Symon C, Arris L, Heal B), pp. 99–150. Cambridge University Press, New York.

Khatami, R., Mountrakis, G., & Stehman, S. V. (2016). A meta-analysis of remote sensing research on supervised pixel-based land-cover image classification processes: General guidelines for practitioners and future research. *Remote Sensing of Environment*, *177*, 89–100. https://doi.org/10.1016/j.rse.2016.02.028

Kohler, J., Brandt, O., Johansson, M., & Callaghan, T. (2006). A long-term Arctic snow depth record from Abisko, northern Sweden, 1913-2004. *Polar Research*, *25*(2), 91–113. https://doi.org/10.1111/j.1751-8369.2006.tb00026.x

Lees, K.J.; Quaife, T.; Artz, R.R.E.; Khomik, M.; Clark, J.M. Potential for using remote sensing to estimate carbon fluxes across northern peatlands – A review. *Science of The Total Environment*, 2018, 615, 857-874. doi.org/10.1016/j.scitotenv.2017.09.103.

Li, M., Zang, S., Zhang, B., Li, S., & Wu, C. (2014). A review of remote sensing image classification techniques: The role of Spatio-contextual information. *European Journal of Remote Sensing*, *47*(1), 389–411. https://doi.org/10.5721/EuJRS20144723

Lu, D. (2006). The potential and challenge of remote sensing-based biomass estimation. *International Journal of Remote Sensing*. https://doi.org/10.1080/01431160500486732

Malmer, N., Johansson, T., Olsrud, M., & Christensen, T. R. (2005). Vegetation, climatic changes and net carbon sequestration in a North-Scandinavian subarctic mire over 30 years. *Global Change Biology*. https://doi.org/10.1111/j.1365-2486.2005.01042.x

Matese, A., Toscano, P., Di Gennaro, S. F., Genesio, L., Vaccari, F. P., Primicerio, J., Gioli, B. (2015). Intercomparison of UAV, aircraft and satellite remote sensing platforms for precision viticulture. *Remote Sensing*, *7*(3), 2971–2990. https://doi.org/10.3390/rs70302971

McCalley, C. K., Woodcroft, B. J., Hodgkins, S. B., Wehr, R. A., Kim, E. H., Mondav, R., … Saleska, S. R. (2014). Methane dynamics regulated by microbial community response to permafrost thaw. *Nature*. https://doi.org/10.1038/nature13798

Mongus, D., & Žalik, B. (2018). Segmentation schema for enhancing land cover identification: A case study using Sentinel 2 data. *International Journal of Applied Earth Observation and Geoinformation*. https://doi.org/10.1016/j.jag.2017.11.004

Olefeldt, D., & Roulet, N. T. (2012). Effects of permafrost and hydrology on the composition and transport of dissolved organic carbon in a subarctic peatland complex. *Journal of Geophysical Research: Biogeosciences*, *117*(1). https://doi.org/10.1029/2011JG001819

Ouma, Y. O., Tetuko, J., & Tateishi, R. (2008). Analysis of co-occurrence and discrete wavelet transform textures for differentiation of forest and non-forest vegetation in very-high-resolution optical-sensor imagery. *International Journal of Remote Sensing*, *29*(12), 3417–3456. https://doi.org/10.1080/01431160701601782

Quinton, W. L., Hayashi, M., & Chasmer, L. E. (2009). Peatland Hydrology of Discontinuous Permafrost in the Northwest Territories: Overview and Synthesis. *Canadian Water Resources Journal*, *34*(4), 311–328. https://doi.org/10.4296/cwrj3404311

Siewart, M.B. High-resolution digital mapping of soil organic carbon in permafrost terrain using machine learning: a case study in a sub-Arctic peatland environment. *Biogeosciences*, 15, 1663-1682. doi.org/10.5194/bg-15-1663-2018

Soares, J. V., Rennó, C. D., Formaggio, A. R., Yanasse, C. D. C. F., & Frery, A. C. (1997). An investigation of the selection of texture features for crop discrimination using SAR imagery. *Remote Sensing of Environment*, *59*(2), 234–247. https://doi.org/10.1016/S0034-4257(96)00156-3

Torbick, N., Persson, A., Olefeldt, D., Frolking, S., Salas, W., Hagen, S., Li, C. (2012). High Resolution Mapping of Peatland Hydroperiod at a High-Latitude Swedish Mire. *Remote Sensing*. https://doi.org/10.3390/rs4071974

Van Der Kolk, H. J., Heijmans, M. M. P. D., Van Huissteden, J., Pullens, J. W. M., & Berendse, F. (2016). Potential Arctic tundra vegetation shifts in response to changing temperature, precipitation and permafrost thaw. *Biogeosciences*, *13*(22), 6229–6245. https://doi.org/10.5194/bg-13-6229-2016